

**OFFICIAL USE ONLY**

Enclosure 1: #58

SANDIA REPORT

SAND88 - 1497  
Printed November 1988

Unique Document # SAB20008780000

# Ground Shock from Earth Penetrator Weapons

Paul Yarrington

CONFIRMED TO BE UNCLASSIFIED  
AUTHORITY DOE/RN-52  
BY R.H. SMILEY  
RHS, ADD, 2-22-96

Prepared by  
Sandia National Laboratories  
Albuquerque, New Mexico 87185 and Livermore, California 94550  
for the United States Department of Energy  
under Contract DE-AC04-76DP00789

CONFIRMED TO BE UNCLASSIFIED  
DOE/OCCIE  
BY: NC Nancy Connelly, Add (DR. 80-10)  
Date: 4/5/05  
HRV/mrb 5/11/07

**OFFICIAL USE ONLY**

8781

Issued by Sandia National Laboratories, operated for the United States Department of Energy by Sandia Corporation.

**NOTICE:** This report was prepared as an account of work sponsored by an agency of the United States Government. Neither the United States Government nor any agency thereof, nor any of their employees, nor any of their contractors, subcontractors, or their employees, makes any warranty, express or implied, or assumes any legal liability or responsibility for the accuracy, completeness, or usefulness of any information, apparatus, product or process disclosed, or represents that its use would not infringe privately owned rights. Reference herein to any specific commercial product, process, or service by trade name, trademark, manufacturer, or otherwise, does not necessarily constitute or imply its endorsement, recommendation, or favoring by the United States Government, any agency thereof or any of their contractors or subcontractors. The views and opinions expressed herein do not necessarily state or reflect those of the United States Government, any agency thereof or any of their contractors.

~~OFFICIAL USE ONLY~~

SAND88-1497  
OFFICIAL USE ONLY  
Printed November 1988

## Ground Shock from Earth Penetrator Weapons

Paul Yarrington  
Computational Physics & Mechanics Division II  
Sandia National Laboratories  
Albuquerque, New Mexico

### ABSTRACT

This report presents results of calculations to predict ground shock effects from earth penetrating weapons. The study models 500 kiloton explosions at two depths below the ground surface in homogeneous, saturated, soft rock geology. Comparisons of weapon lethal range are made using various free-field damage criteria for near-surface and deeply-buried targets. Comparisons are also made with calculational results for ground shock from above-surface and shallowly-buried selected bursts.

~~OFFICIAL USE ONLY~~

## Contents

<b>1. Introduction</b>	<b>1</b>
<b>2. Calculational Approach</b>	<b>2</b>
<b>3. Calculational Results and Description of Phenomenology</b>	<b>7</b>
<b>4. Comparison of Ground Shock Effects</b>	<b>17</b>
<b>5. Discussion</b>	<b>29</b>
<b>6. Acknowledgements</b>	<b>30</b>
<b>7. References</b>	<b>31</b>
<b>APPENDIX</b>	<b>32</b>

## List of Figures

1	Hugoniot curves for wet tuff model. . . . .	3
2	Hugoniot and release curves for wet tuff model. ( $P_r$ is the shock pressure from which release occurs.) . . . . .	4
3	One megabar pressure contour for 6m DOB EPW at 50 $\mu$ sec. . . . .	9
4	Sequence of early time pressure contours for 6m DOB EPW. . . . .	10
5	Velocity and temperature profiles on axis for 6m DOB EPW. . . . .	11
6	Energy partitioning between ground and air for 6m DOB EPW. . . . .	12
7	Pressure contours for 6m DOB EPW and 12m DOB EPW. . . . .	13
8	Energy history in air for EPW bursts. . . . .	14
9	Pressure decay at center of burst for EPW and fully-contained explosions. . . . .	15
10	Late-time pressure contours for EPW bursts. . . . .	16
11	Comparison of 0.5 kb peak axial stress contours for EPW bursts. . . . .	18
12	Comparison of 1.0 kb peak axial stress contours for EPW bursts. . . . .	19
13	Comparison of 0.5 kb peak axial stress contours for above-surface and EPW bursts. . . . .	20
14	Comparison of 1.0 kb peak axial stress contours for above-surface and EPW bursts. . . . .	21
15	Peak stress on axis versus depth for EPW bursts and fully-contained explosion. . . . .	24
16	Peak stress attenuation on axis for EPW and near-surface bursts. . . . .	25
17	Yield factor as function of burst position. . . . .	26
18	Comparison of 6 m/s peak horizontal velocity contours for EPW bursts. . . . .	27
19	Comparison of 0.5 kb peak horizontal stress contours for EPW bursts. . . . .	28

## 1. Introduction

This report presents results of calculations done to study ground shock formation and propagation from buried explosions. The work was part of a broader calculational study involving above-surface, as well as, below-surface bursts. The purpose of the study was to understand the influence of burst position on high-yield weapon effects against hardened, military targets. The present report discusses calculations of earth penetrator weapon (EPW) effects, where the bursts are at significant depths below the surface. The companion calculations in this study for near-surface bursts are discussed in detail elsewhere (see, [1], [2]); however, selected results of those calculations are compared here with ground shock effects predicted for EPW bursts.

A 500 kiloton source was modeled in this study, with the initial energy density of the explosion being representative of a nuclear burst. The calculations simulate bursts at 6 meters and 12 meters below the ground surface, depths believed achievable by a strategic earth penetrating weapon (EPW) in typical, near-surface geologic media. The target material was assumed to be a homogeneous, infinitely-deep layer (half-space) of wet soft rock, with material properties chosen to model saturated, ash-fall tuff. Both the weapon yield and target geology were chosen to be the same as were used for the near-surface burst calculations in the companion studies [1,2] in order to facilitate ground shock comparisons between the various cases.

The initial assumptions and zoning philosophy used in the calculations are described in Section 2. Section 3 presents calculational results which illustrate the phenomenology predicted for the EPW bursts. In Section 4, ground shock lethal radii for the 6 and 12 meter depth EPW bursts are compared, using typical hard target damage criteria. Comparisons are also shown between the predicted ground shock effects for the EPW bursts and those associated with near-surface bursts, as described in [1] and [2].

## 2. Computational Approach

The calculations reported here were performed with the two-dimensional, Eulerian wavecode, CSQII (version 6/82) [3], assuming cylindrical symmetry about the penetrator axis. The penetrator was modeled as a solid cylinder of iron, 30 cm in diameter and 180 cm long. The center of the penetrator was assumed to be at the nominal depth of burst for each problem. Energy release for the the EPW burst was simulated by uniformly depositing 500 kt ( $2.1 \times 10^{22}$  ergs) of energy in the iron cylinder representing the penetrator, with the energy being deposited at a constant rate over a time interval of 20 nanoseconds.

The effects of the penetration event on the target material above the weapon were assumed to be of negligible importance to the energy coupling and ground shock associated with the EPW bursts. Thus, the target medium surrounding the weapon in all directions was modeled as uniform and undisturbed. Air above the ground surface was explicitly modeled in the calculations.

The ANEOS [4] equation-of-state (EOS) package associated with CSQ was used to model the materials in the calculations. A library EOS (ANEOS Library Material No. -5) was used for the iron penetrator, although, given the extremely high temperatures reached by the penetrator materials, the ground shock effects are essentially independent of the material chosen to model the projectile. A tabular EOS (Table No. 1885) was used for the air. The ANEOS input for the tuff is given in Appendix 1, while principal material properties are listed in Table 1. Material properties for the tuff were chosen to be the same as those used in an earlier Sandia calculational study [5] of ground shock effects. Hugoniot and selected release curves generated with the tuff model are shown in Figures 1 and 2.

OFFICIAL USE ONLY

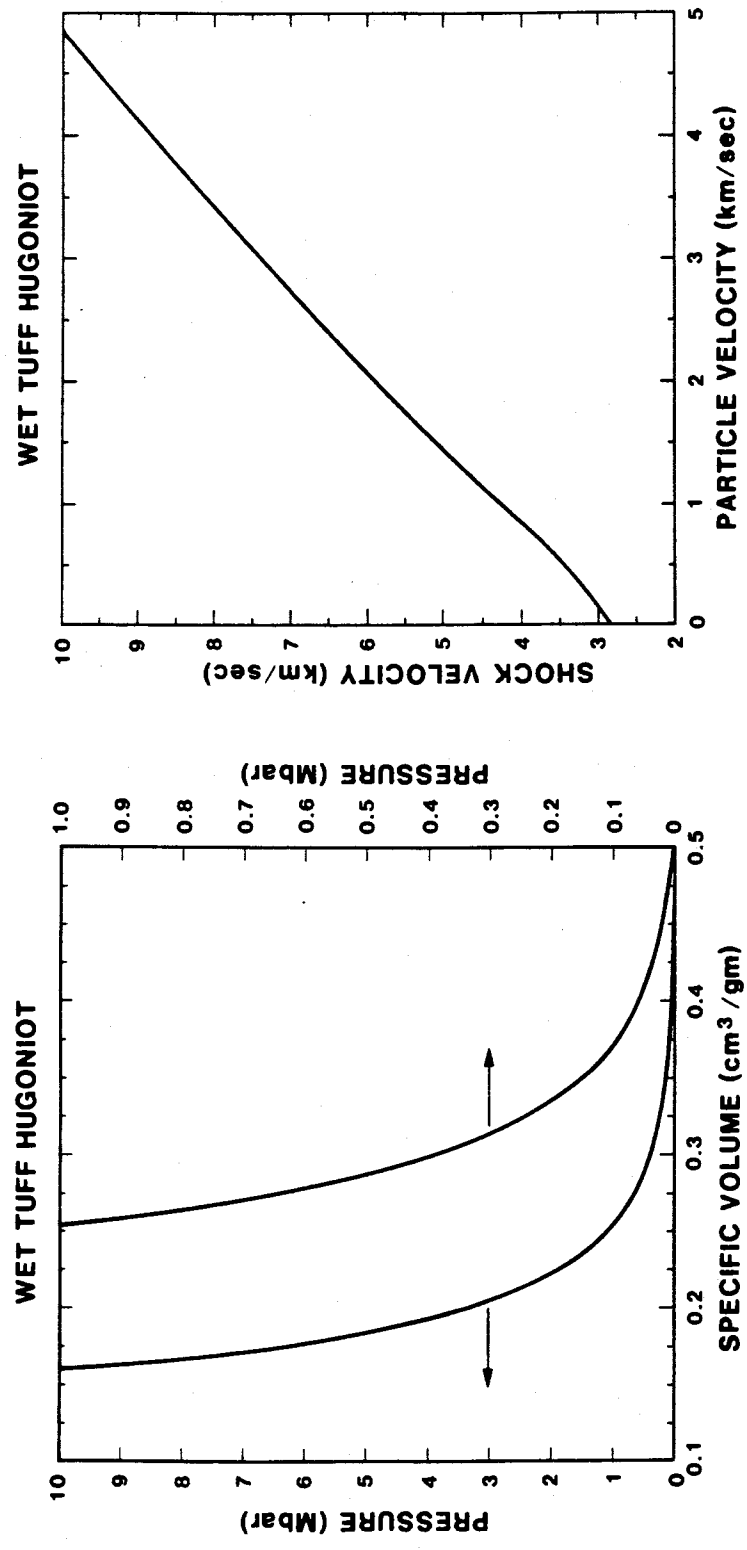


Figure 1: Hugoniot curves for wet tuff model.

OFFICIAL USE ONLY

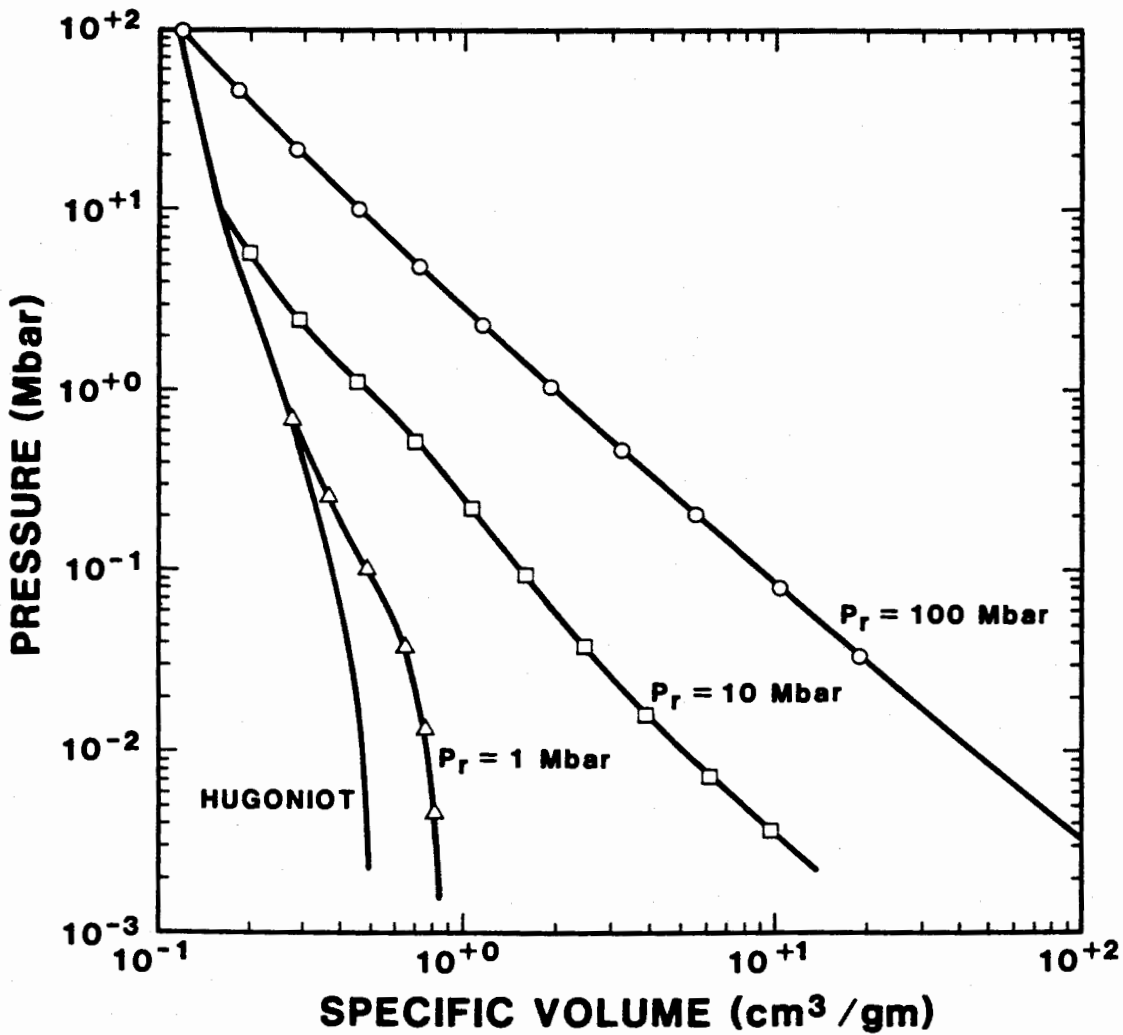


Figure 2: Hugoniot and release curves for wet tuff model. (P<sub>r</sub> is the shock pressure from which release occurs.)

Property	Symbol	Value
Initial Density	$\rho_0$	2.0 gm/cc
Sound speed	$C_0$	$2.8 \times 10^5$ cm/sec
Poisson's ratio	$\mu$	0.31
Mises limit	$Y_m$	0.3 Kbar
Yield constant	$k$	$3.1 \text{ Kbar}^{-1}$

The yield strength for the tuff was assumed to be pressure-dependent, with the yield surface having the form

$$Y(P) = Y_m(1 - e^{-kP}) .$$

The strength constants  $Y_m$  and  $k$  used for the tuff are given in Table 1. The pressure,  $P$ , in this relation is calculated from

$$P = \rho c^2 \eta ,$$

where  $\rho$  and  $c$  are, respectively, the current density and sound speed of the material, and

$$\eta = 1 - \rho_0/\rho .$$

The deviatoric stress state in the material is limited by the yield surface,  $Y(P)$ , calculated from the relation above, as described in Sect. II-4 of the CSQ documentation [3]. Since this pressure-dependent strength model is not a standard option in CSQ, the updates that were used to implement it in the code are included in the Appendix.

The initial zoning for the problem employed uniform, 5 cm square zones, to a radius of 5 meters (100 zones) from the center of the explosion. Shortly before the shock wave from the burst reached the edge of the initial mesh, the problem was rezoned by doubling the zone size and the overall dimensions of the calculational grid. This zoning/rezoning approach, in which square zones are used in the ground shock region, with 100 zones in each direction (horizontally outward and vertically downward) from

the burst, and in which the zone size is doubled when the disturbance reaches the edge of the mesh, was used throughout the calculations. The procedure provides a minimum of 50 zones between the original center of the burst and the leading edge of the ground shock at all times during the calculations. Above the ground surface, zones were allowed to increase in vertical dimension by a constant ratio (always less than 5 percent) as the vertical distance increased. The calculations were rezoned eight times, as indicated in Table 2, to reach the final problem time of 0.3 seconds.

**TABLE 2**

**Zoning for EPW Calculations**

Time	Shock Radius	Zone Size*
0 - 30 usec	0 - 5 m	5 cm
30 - 200 usec	5 - 10 m	10 cm
200 - 800 usec	10 - 20 m	20 cm
0.8 - 4 ms	20 - 40 m	40 cm
4 - 12 ms	40 - 80 m	80 cm
12 - 35 ms	80 - 160 m	160 cm
35 - 80 ms	160 - 320 m	320 cm
80 - 175 ms	320 - 640 m	640 cm

\*Zone size refers to side length in square-zoned region of mesh extending 100 zones horizontally outward and 100 zones vertically downward from the center of burst.

### 3. Calculational Results and Description of Phenomenology

Within a few microseconds after the burst, the expanding cavity of vaporized tuff and weapon debris becomes essentially spherical. This can be seen in Figure 3, which shows the 1 Mbar pressure contour for the 6 m DOB problem at 50 microseconds, shortly before the burst breaks through the surface of the ground. Note that the center of burst was at the origin of the coordinate system in both of the EPW calculations. When breakout occurs, energy is rapidly lost from the cavity, as hot, high pressure gases vent to the atmosphere. Figure 4 shows a sequence of early-time pressure contours, where the strong hydrodynamic motions that occur following breakout are evident. Velocity and temperature profiles on axis during this cavity breakout phase of the problem are shown in Figure 5. Histories of total energy in the tuff and in the air are cross-plotted to a problem time of 10 ms in Figure 6, where the rapid, early-time transfer of energy from tuff to air can be clearly seen.

For the deeper burst, these processes occur later in time, and less energy is transferred to the air than for the shallower burst. Figure 7 compares pressure contours for the two EPW bursts at problem times of 2 ms, 6 ms and 10 ms. Figure 8 shows the time history of total energy in the air during the first 30 ms for the two problems. As time progresses, the pressure in the cavity for both bursts drops well below that for a fully-contained explosion [6], as shown in Figure 9.

Figure 10 compares late-time pressure contours for both problems and shows a somewhat stronger ground shock for the deeper burst, as would be expected. This is evident from the wider contours that are seen for the deeper burst at any given stress level. Compare, for example, the 0.5 kb contours (level E) for the two cases.

With the contour levels chosen in Figure 10, the front of a pressure wave can be seen propagating in the air along the ground surface, suggesting that some "airblast" effects may be associated with the EPW bursts. The strength of this blast wave is

OFFICIAL USE ONLY

greatly reduced, however, from that produced by a surface burst and will decay to negligible levels at ranges where the ground shock is still well above its lethal level. Thus, ground shock is definitely the dominant weapon effect against hardened structures for the EPW bursts simulated here, with "airblast" making virtually no contribution to the overall lethal radius of the weapon.

OFFICIAL USE ONLY

OFFICIAL USE ONLY

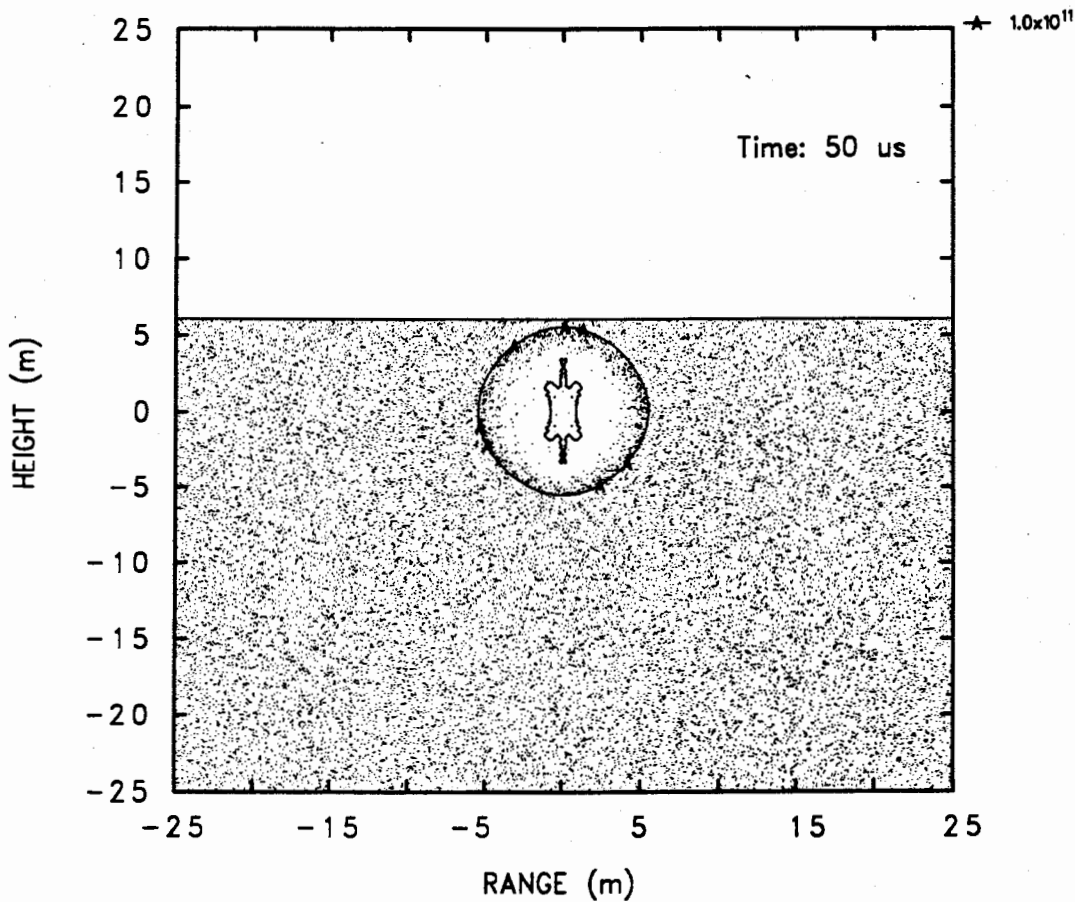


Figure 3: One megabar pressure contour for 6m DOB EPW at 50  $\mu$ sec, shortly before cavity breakout. (Note: Center of burst is at the origin.)

OFFICIAL USE ONLY

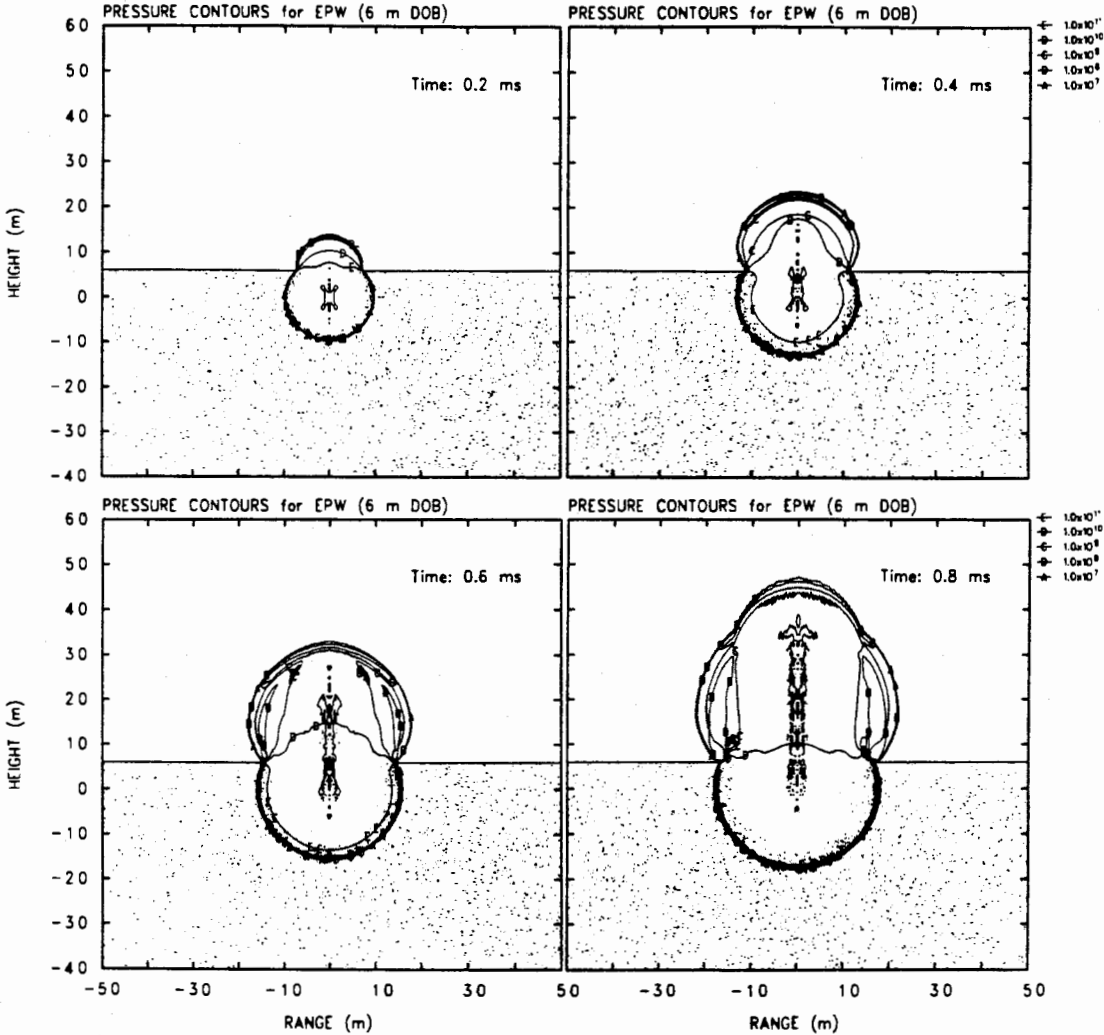


Figure 4: Sequence of early time pressure contours for 6m DOB EPW, showing rapid venting from cavity to air. Contour levels (in Pa) indicated at the right.

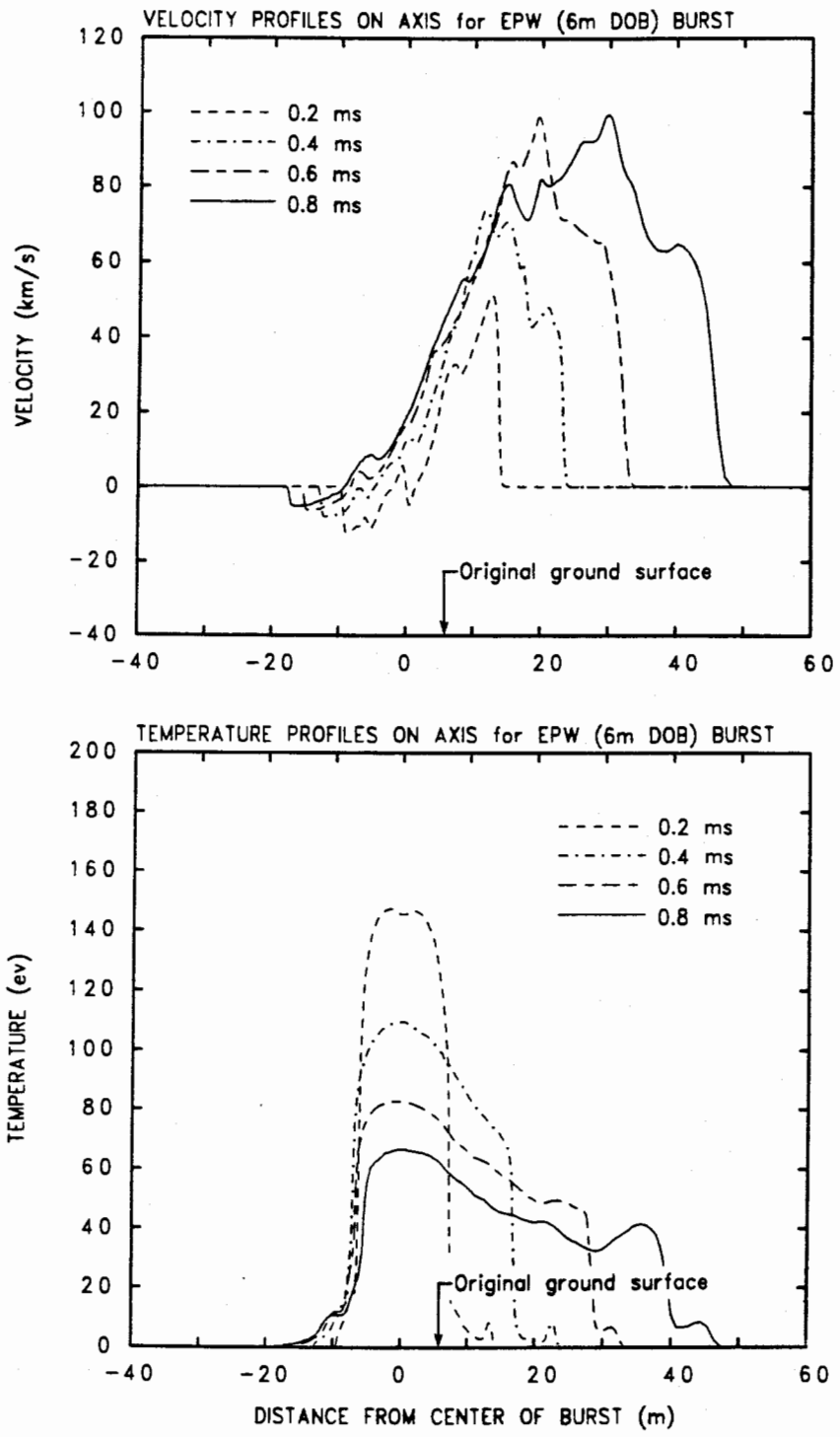


Figure 5: Velocity and temperature profiles on axis for 6m DOB EPW during cavity venting phase of problem.

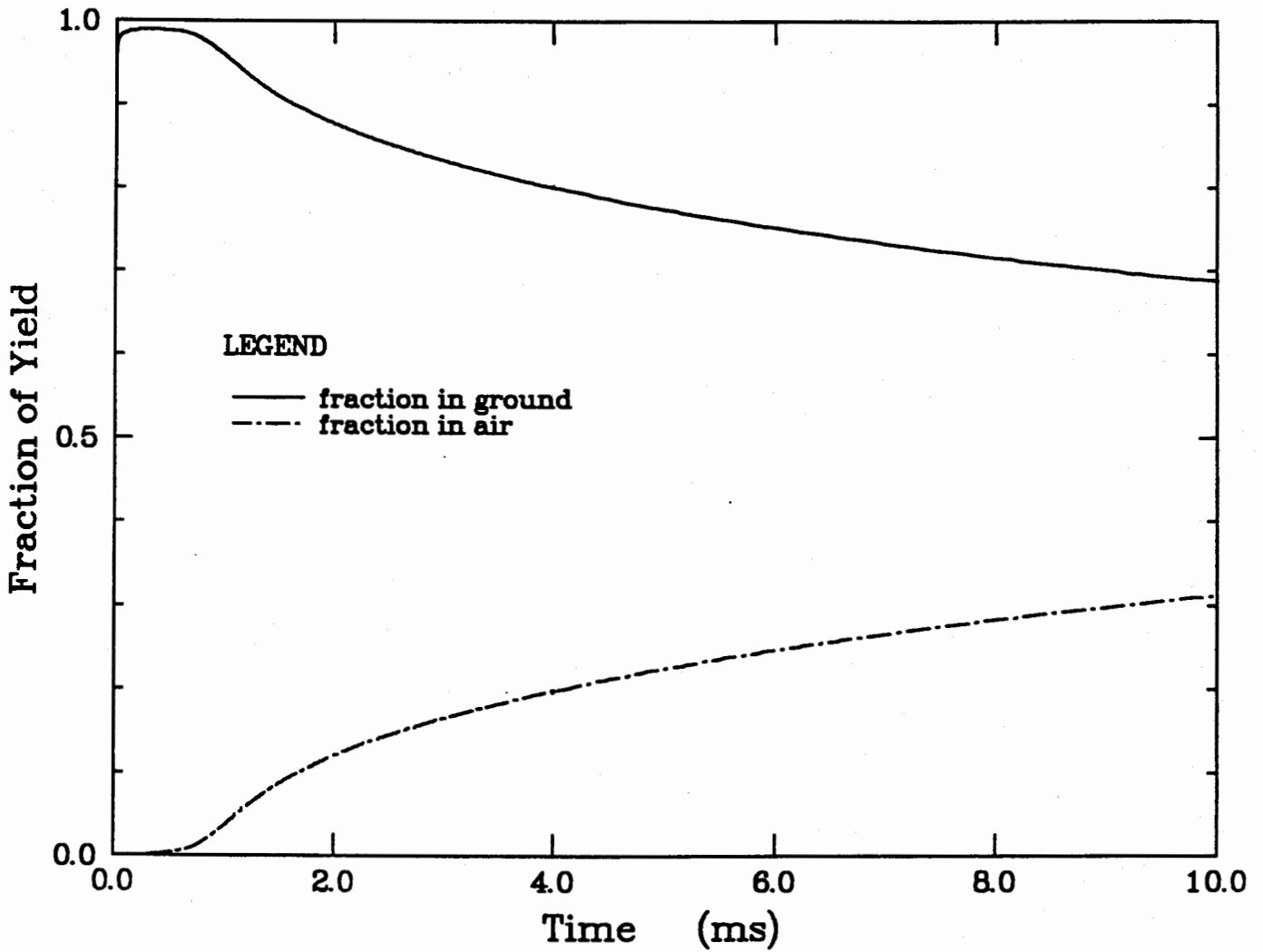


Figure 6: Energy partitioning between ground and air for 6m DOB EPW.

OFFICIAL USE ONLY

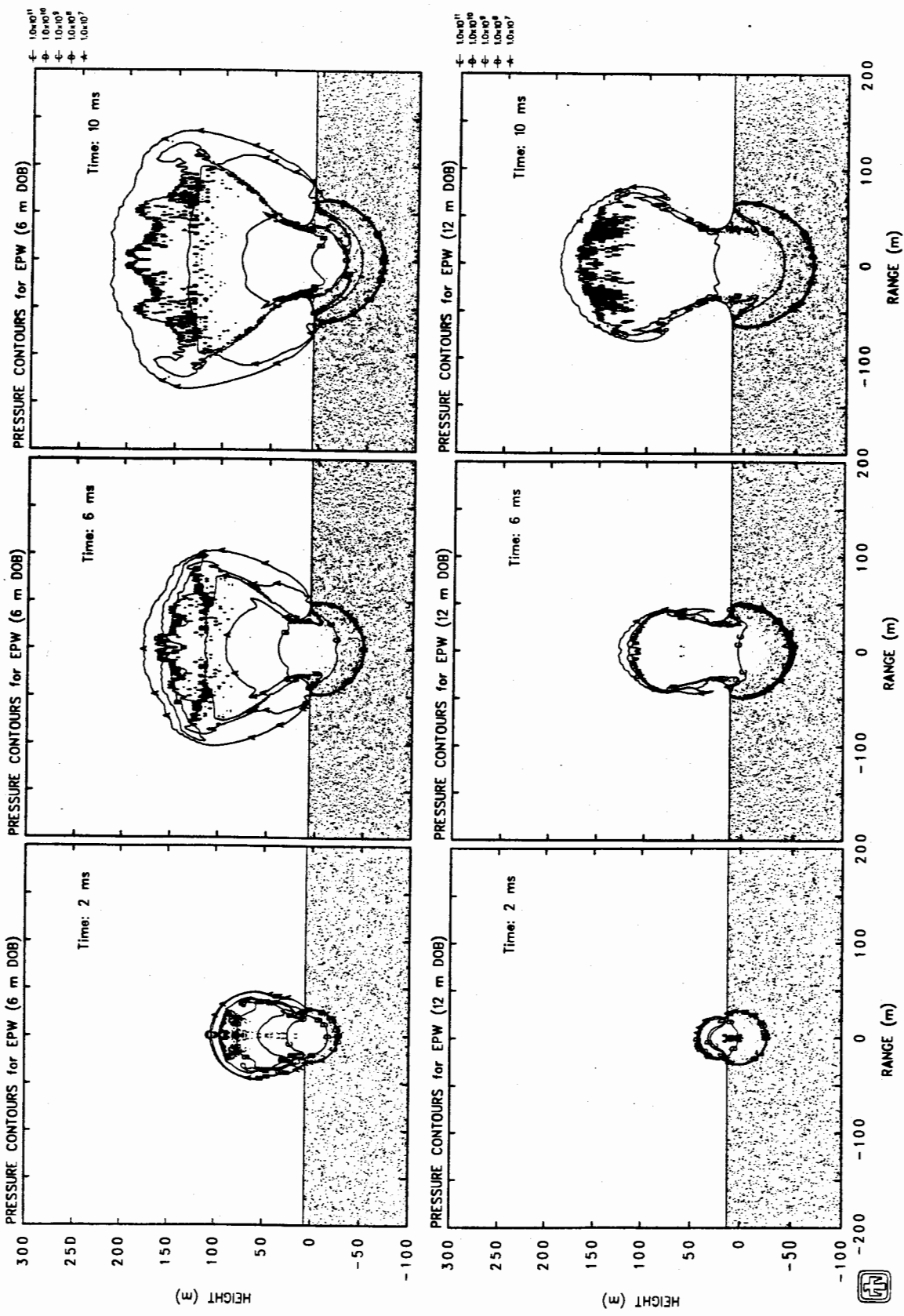


Figure 7: Pressure contours for 6m DOB EPW (top row) and 12m DOB EPW (bottom row). Contour levels (in Pa) indicated at top right.

OFFICIAL USE ONLY

OFFICIAL USE ONLY

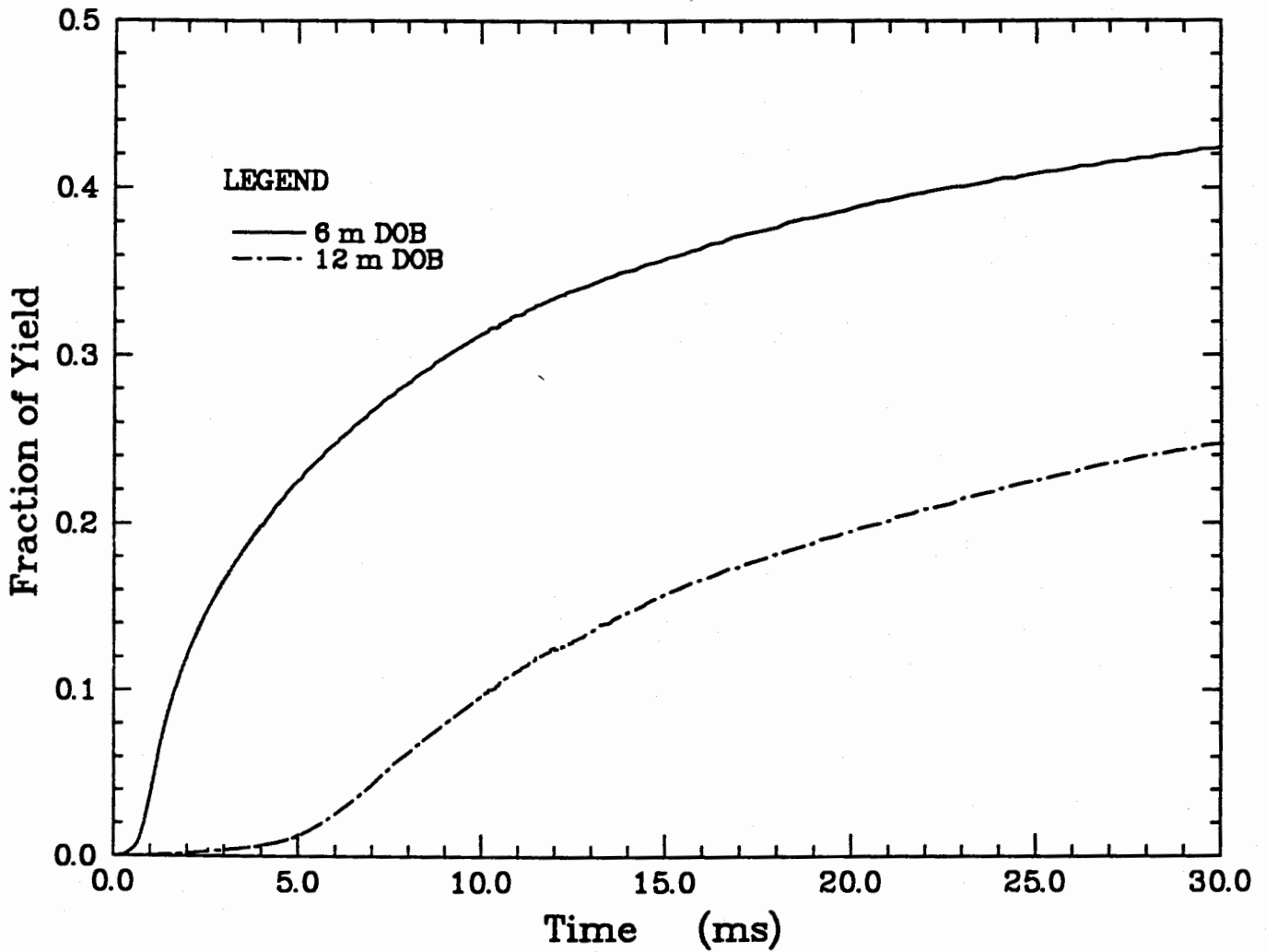


Figure 8: Energy history in air for EPW bursts.

OFFICIAL USE ONLY

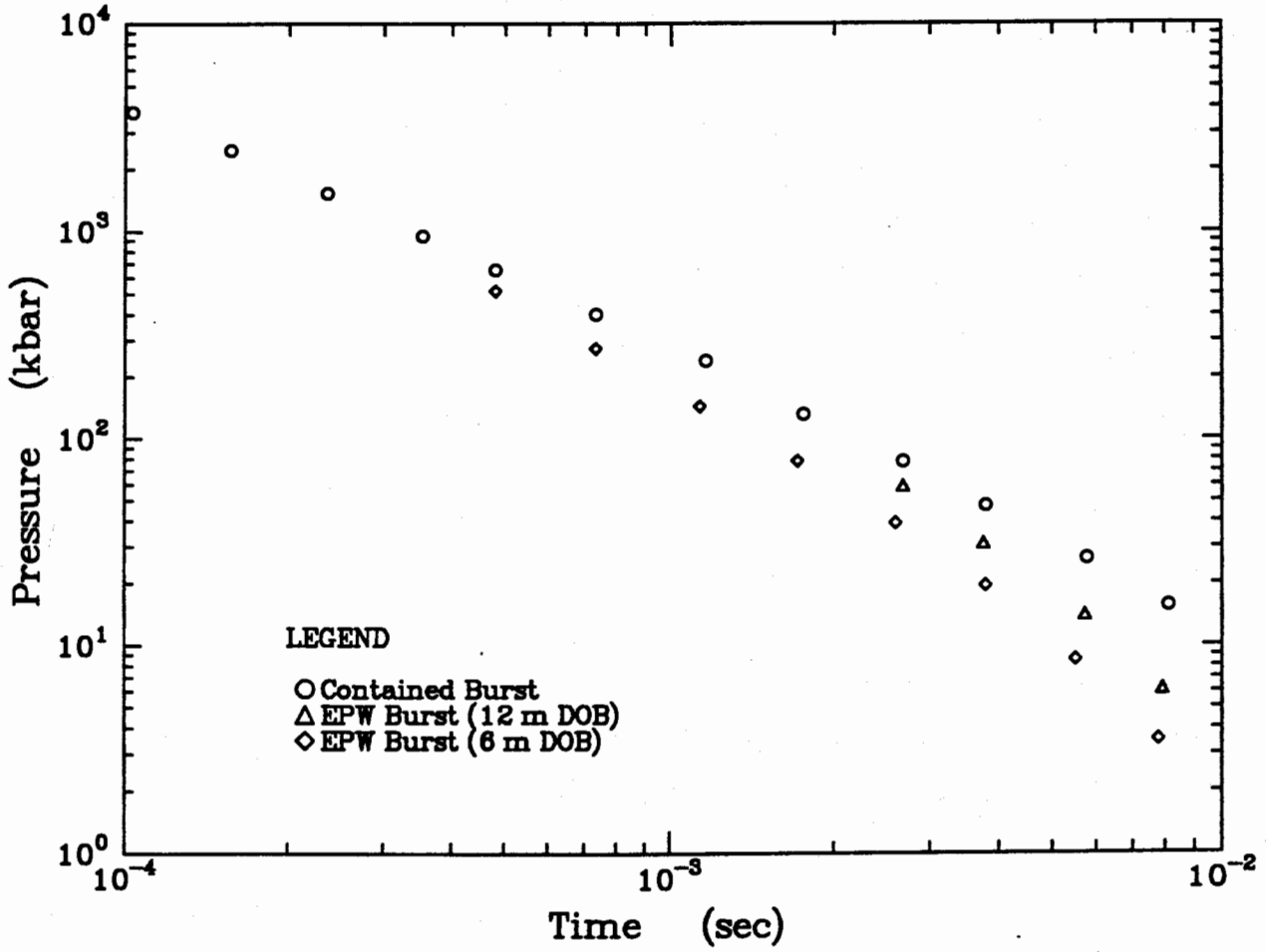


Figure 9: Pressure decay at center of burst for EPW and fully-contained explosions.

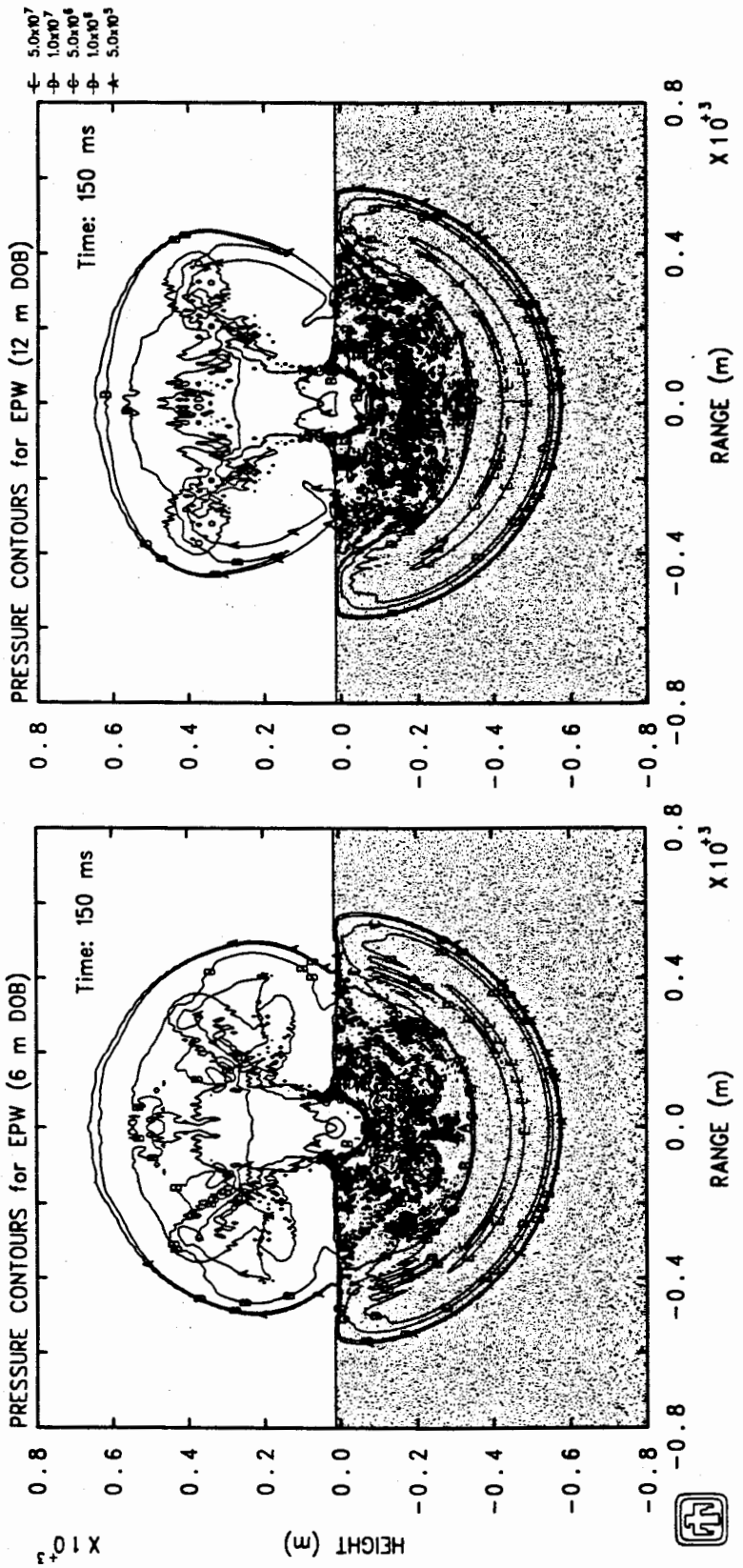


Figure 10: Late-time pressure contours for EPW bursts. Contour level (in Pa) indicated at right. (Note: Center of burst is at the origin in both cases.)

#### 4. Comparison of Ground Shock Effects

Peak ground shock quantities were monitored throughout the computational grid in each calculation, so that direct, quantitative comparisons could be made of the regions subjected to any particular level of free-field stress or velocity. In particular, peak values of stress and particle velocity were monitored in both the horizontal and vertical directions at each point in the mesh. The updates used in CSQ to save these quantities are listed in the Appendix.

For evaluating weapon effects against deeply-buried strategic targets, peak axial stress is the ground shock quantity of interest, and it is widely believed that a peak axial stress in the range of 0.5 kb to 1.0 kb would be required to cause severe structural damage. Accordingly, Figure 11 compares the 0.5 kb peak axial stress contours for the two EPW bursts. Notice that an additional 6 meters in depth-of-burst produces an additional 80 meters in depth-to-effect (*i.e.*, depth to which 0.5 kb peak axial stress is delivered below the burst). The 1.0 kb peak axial stress contours for the two bursts are compared in Figure 12.

It should be noted that the peak stress contours in Figures 11 and 12 display reduced range-to-effect closer to the surface, where the shock front is more highly attenuated by stress release waves from the air/ground interface.

It is of interest to compare ground shock effects from the EPW bursts with those from near-surface bursts. Figure 13 shows, again, the 0.5 kb peak axial stress contours for the EPW bursts, together with the corresponding contours for a shallowly-buried burst (DOB: 1.15 m), a contact burst (HOB: 0.5 m), and a proximity burst (HOB: 6.0 m), as reported in References [1] and [2]. The 1.0 kb peak axial stress contours for the various bursts are shown in Figure 14. It should be noted from these comparisons that even relatively small depths of burial for a high-yield nuclear explosion can produce significant enhancement in ground shock effects.

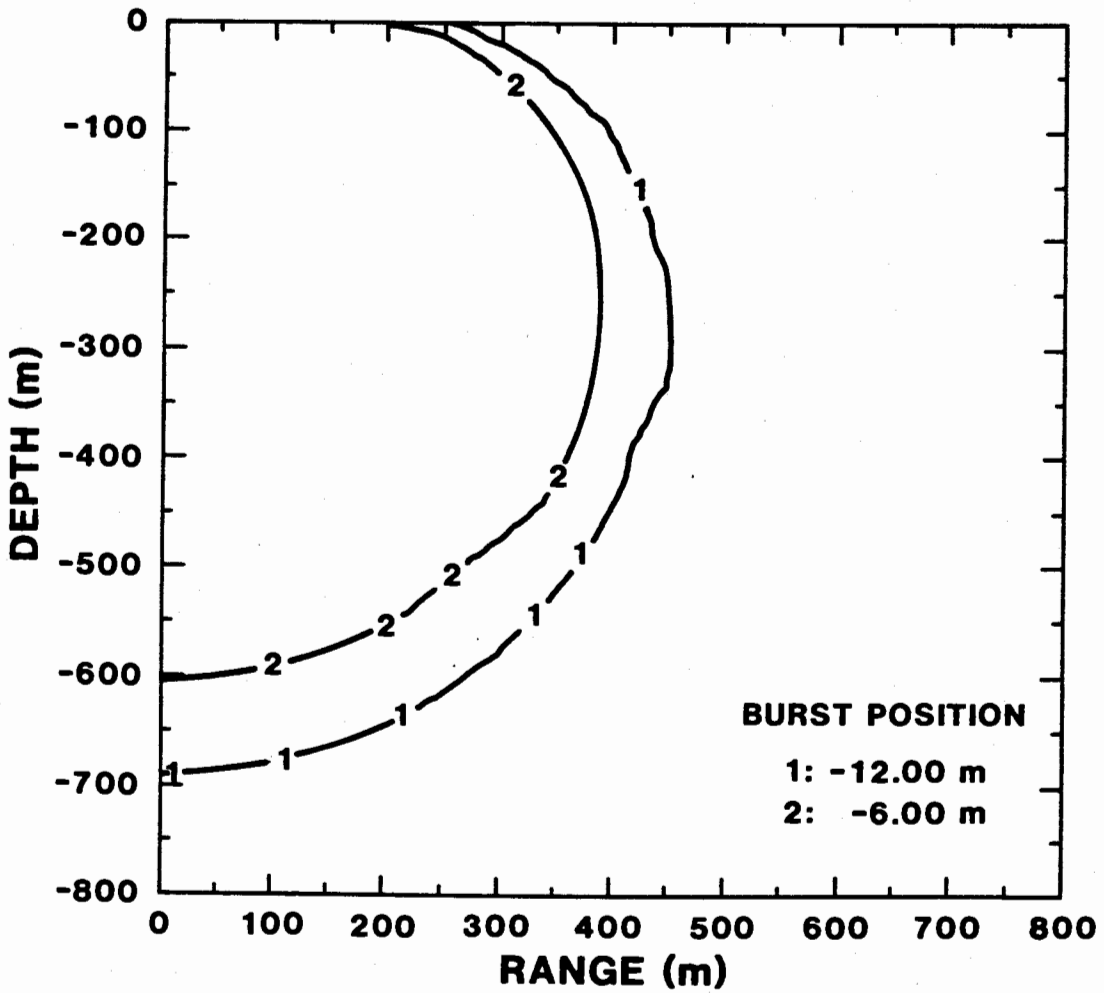


Figure 11: Comparison of 0.5 kb peak axial stress contours for EPW bursts.

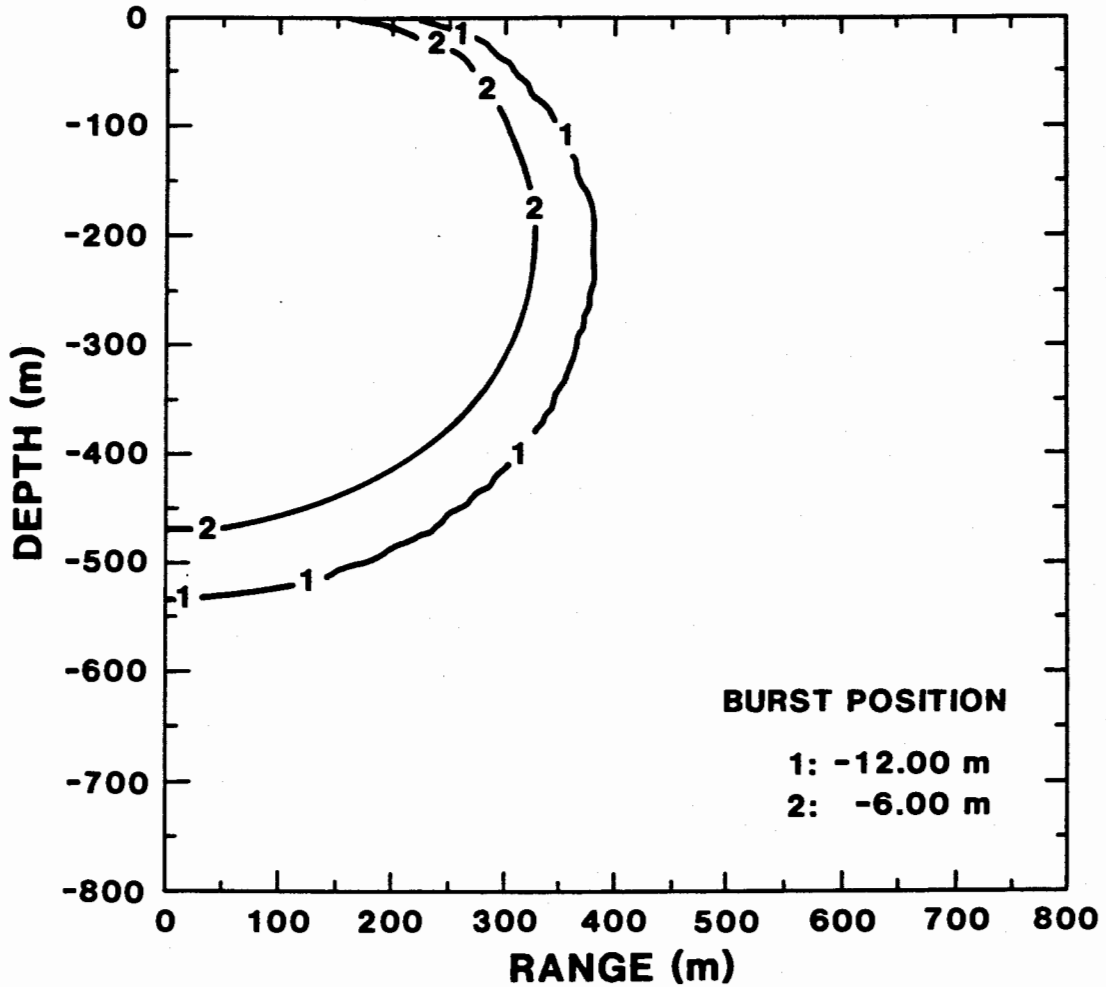


Figure 12: Comparison of 1.0 kb peak axial stress contours for EPW bursts.

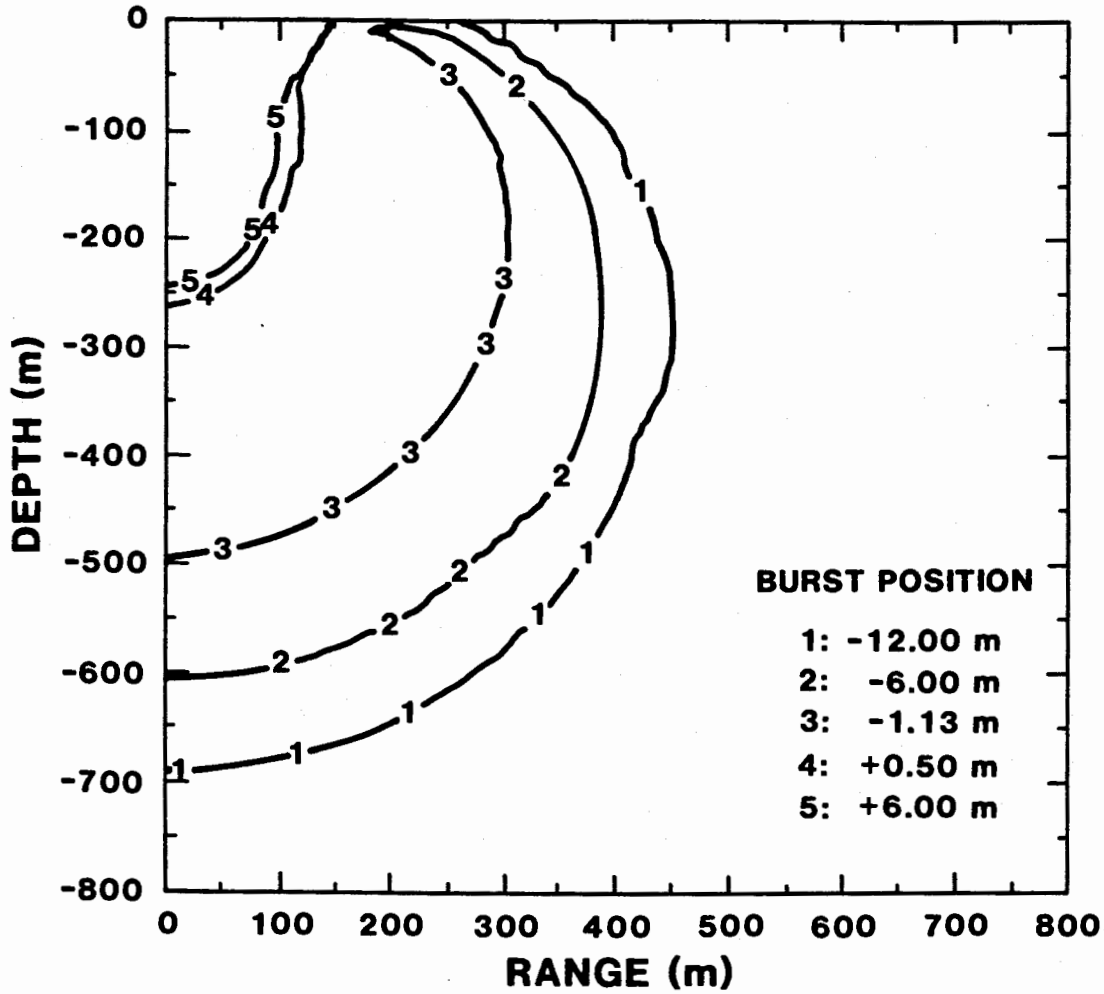


Figure 13: Comparison of 0.5 kb peak axial stress contours for above-surface and EPW bursts.

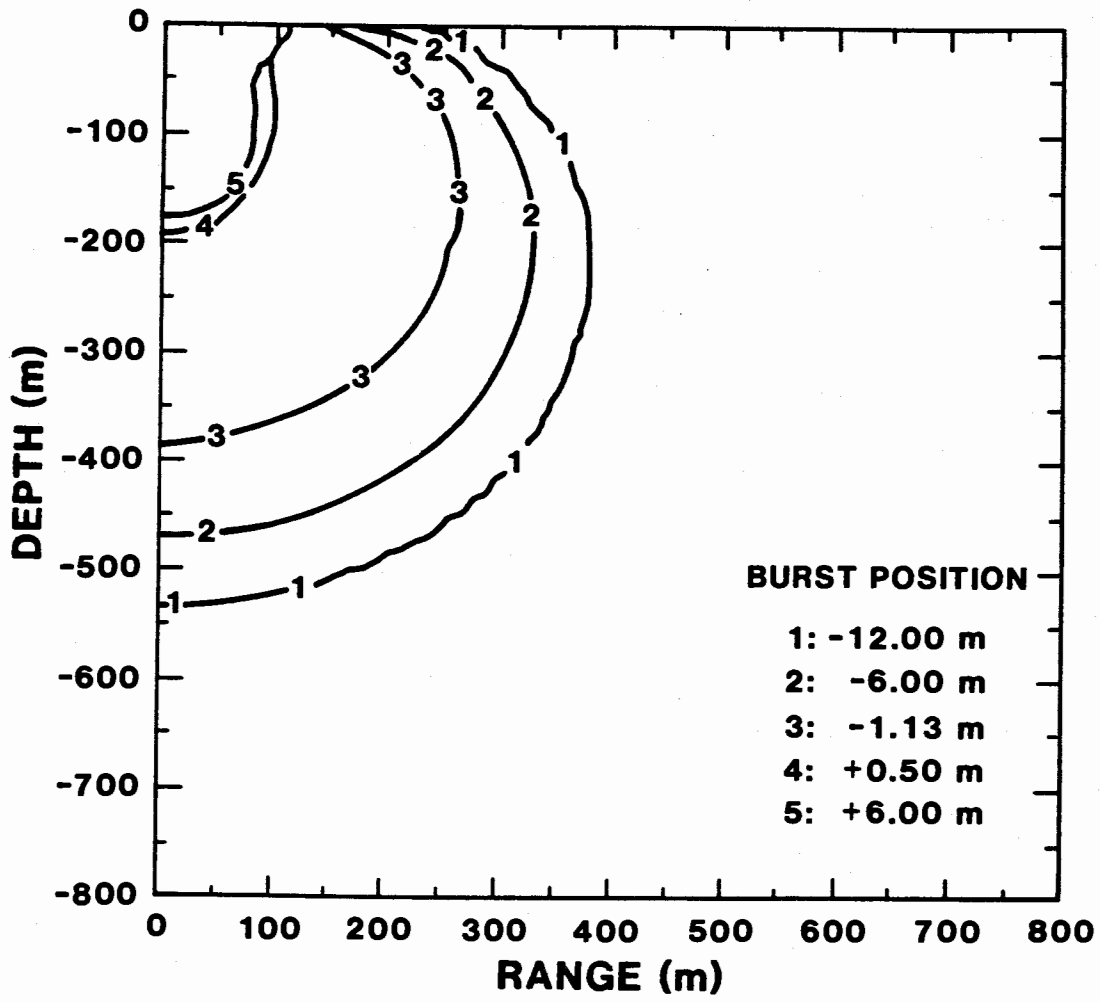


Figure 14: Comparison of 1.0 kb peak axial stress contours for above-surface and EPW bursts.

Peak axial stress for the two EPW bursts is plotted versus depth below burst in Figure 15. The higher stress attenuation rate seen for the shallower burst reflects the fact that the rate, and total amount, of energy lost to the air increases as depth of burst decreases. The stress attenuation curve for a calculation of a fully-contained explosion [6] is also shown in Figure 15, for comparison with the EPW results. The fully-contained burst represents the limiting case of ground shock energy coupling efficiency, since no energy is lost to the air for this problem. The results shown in Figure 15 clearly indicate that increasing the depth of burst beyond 12 m would lead to increased ground coupling efficiency for the EPWs, i.e., higher peak stress levels at a given range from the explosion.

Figure 16 replots the results shown in Figure 15 on a larger, logarithmic scale, along with the corresponding stress attenuation curves for the near-surface bursts (see Ref. [1] and [2]) mentioned above. Using well-established cube-root-scaling rules for ground shock (see, e.g., Section V in Ref. [7]), together with the results shown in Figure 16, yield enhancement factors can be calculated for the relative coupling efficiency of the various bursts at particular levels of peak ground shock stress. Figure 17 shows a plot of yield factor, normalized to results for the contact burst, based on the results shown in Figure 16. Using the 0.5 kb peak axial stress level for illustration, we see that the yield factor for the EPW at 12 m DOB is 18. In other words, the EPW burst of 500 Kt delivers 0.5 kb peak axial stress to a depth below the burst that would require a 9 Mt contact burst, i.e., a contact burst 18 times greater in yield than the EPW. Notice, also, that the EPW yield effectiveness is reduced by 30 percent if the DOB is reduced to 6 m, and is reduced an additional 30 percent, approximately, if the DOB is only 1 meter below the surface.

For near-surface targets, such as missile silos, peak horizontal velocity or peak horizontal stress are more appropriate measures for evaluating ground shock effects. The complete 6 m/s peak horizontal velocity contours for the two EPW bursts are shown in Figure 18, for illustrative purposes, and can be compared with similar results

obtained for near-surface bursts in the companion studies [1,2]. Note the roughly horizontal "airblast wing" near the ground surface for the 6 m DOB case. The similar, but smaller, airblast effect for the 12 m deep burst does not extend far enough into the target to be seen in Figure 18, since the center of burst was at (0,0) in both EPW calculations. Peak axial stress contours at the 0.5 kilobar level are shown in Figure 19. It will be noted that both the 6 m/s peak horizontal velocity contours shown in Figure 18 and the 0.5 kilobar peak horizontal stress contours shown in Figure 19 extend to approximately the same maximum range from the burst.

It should be noted that, in many cases, the near surface geology for realistic land-based targets is likely to consist of softer, more porous material than the wet tuff modeled in this study. Such material would be more dissipative than the tuff, and the ground shock would attenuate more rapidly than was seen in the calculations here. However, we do not expect the *relative* effectiveness against near-surface targets of EPW bursts, at the two depths considered in the present study, to be particularly sensitive to the geology.

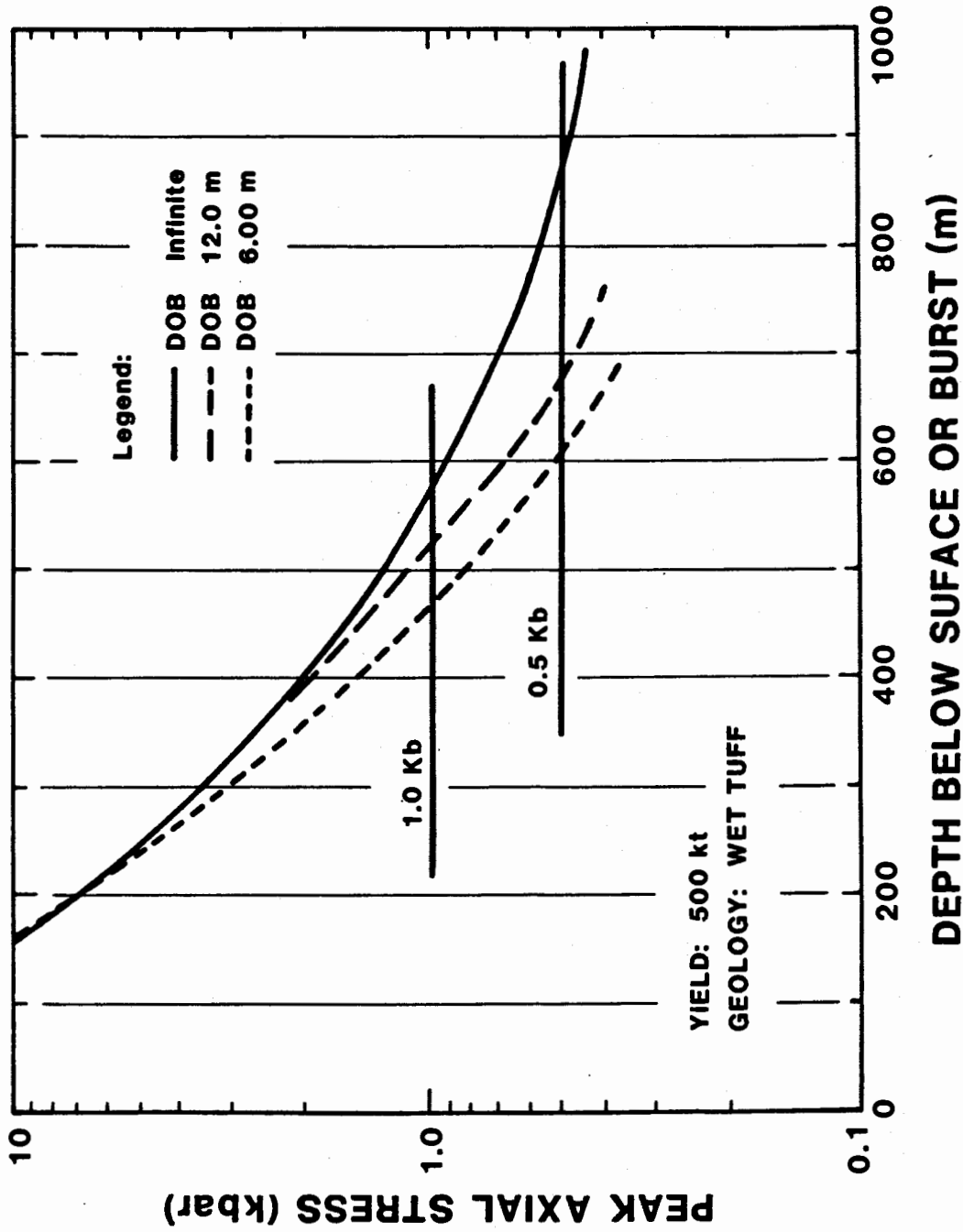


Figure 15: Peak stress on axis versus depth for EPW bursts and fully-contained explosion.

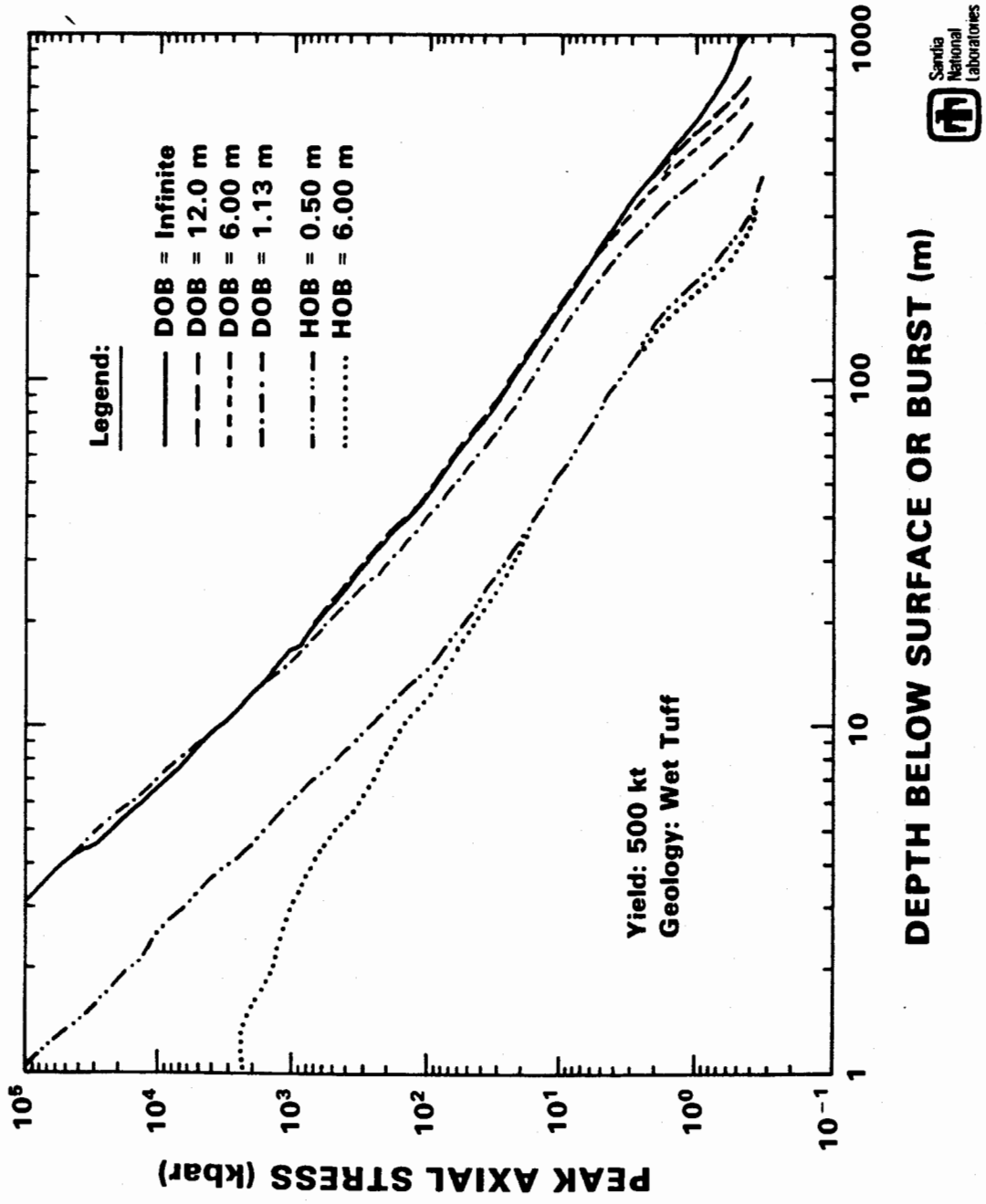


Figure 16: Peak stress attenuation on axis for EPW and near-surface bursts.

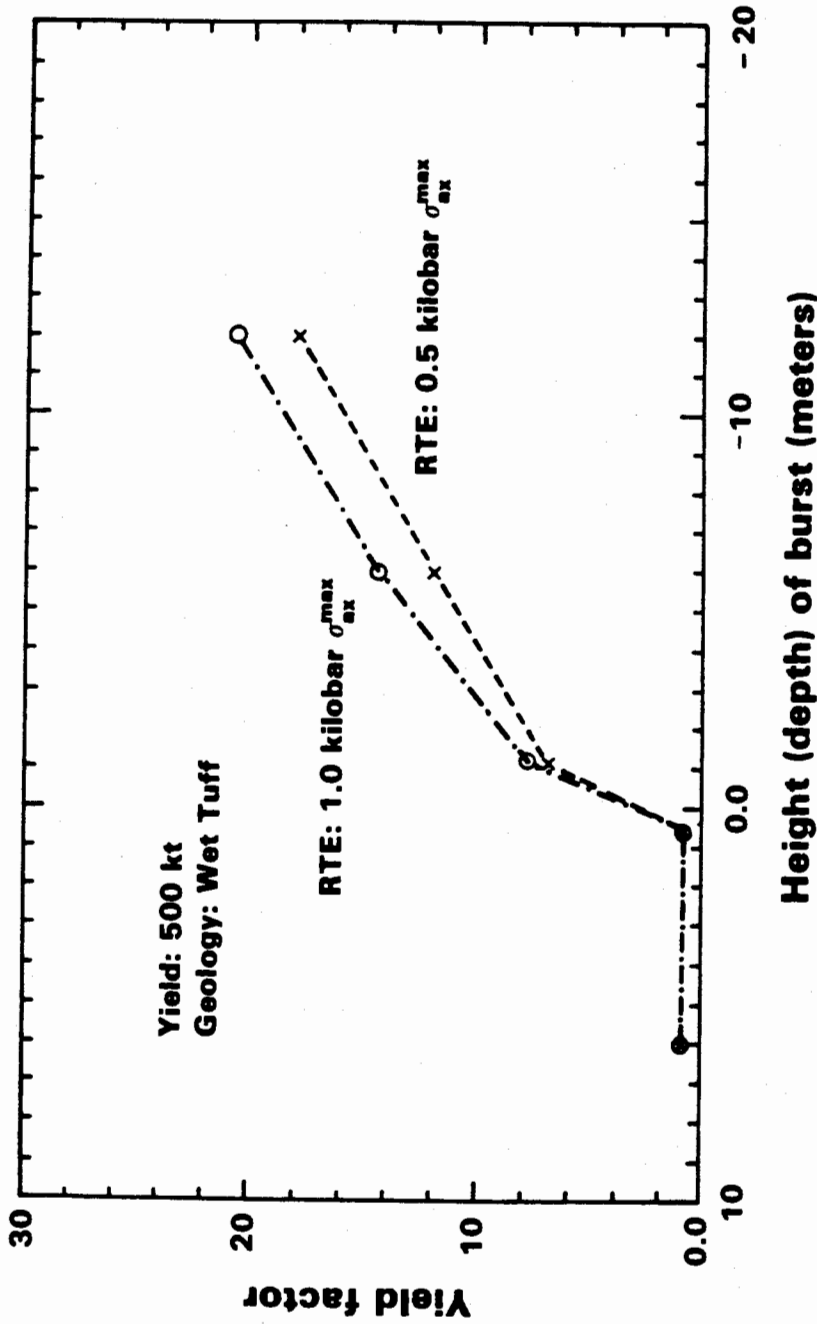


Figure 17: Yield factor (normalized to contact burst) as function of burst position.

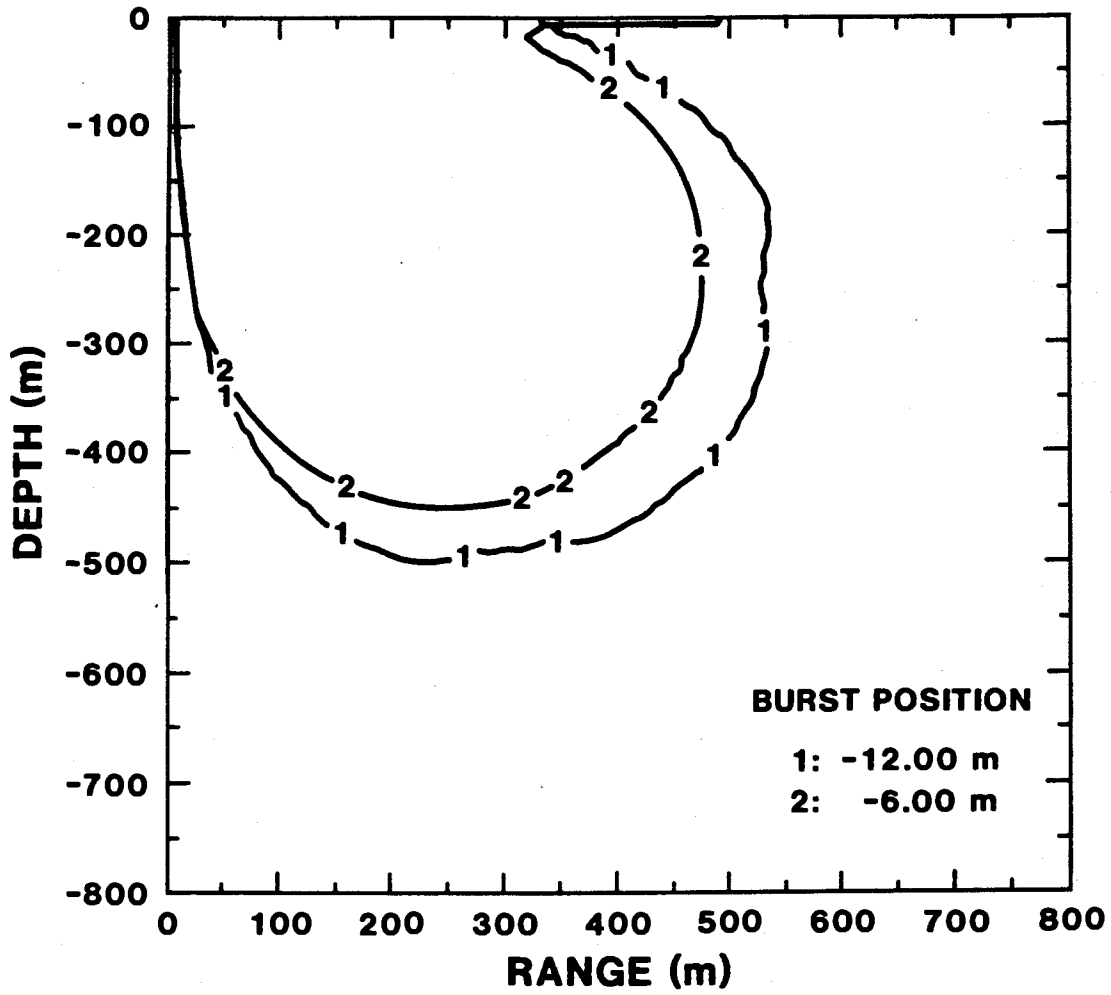


Figure 18: Comparison of 6 m/s peak horizontal velocity contours for EPW bursts.

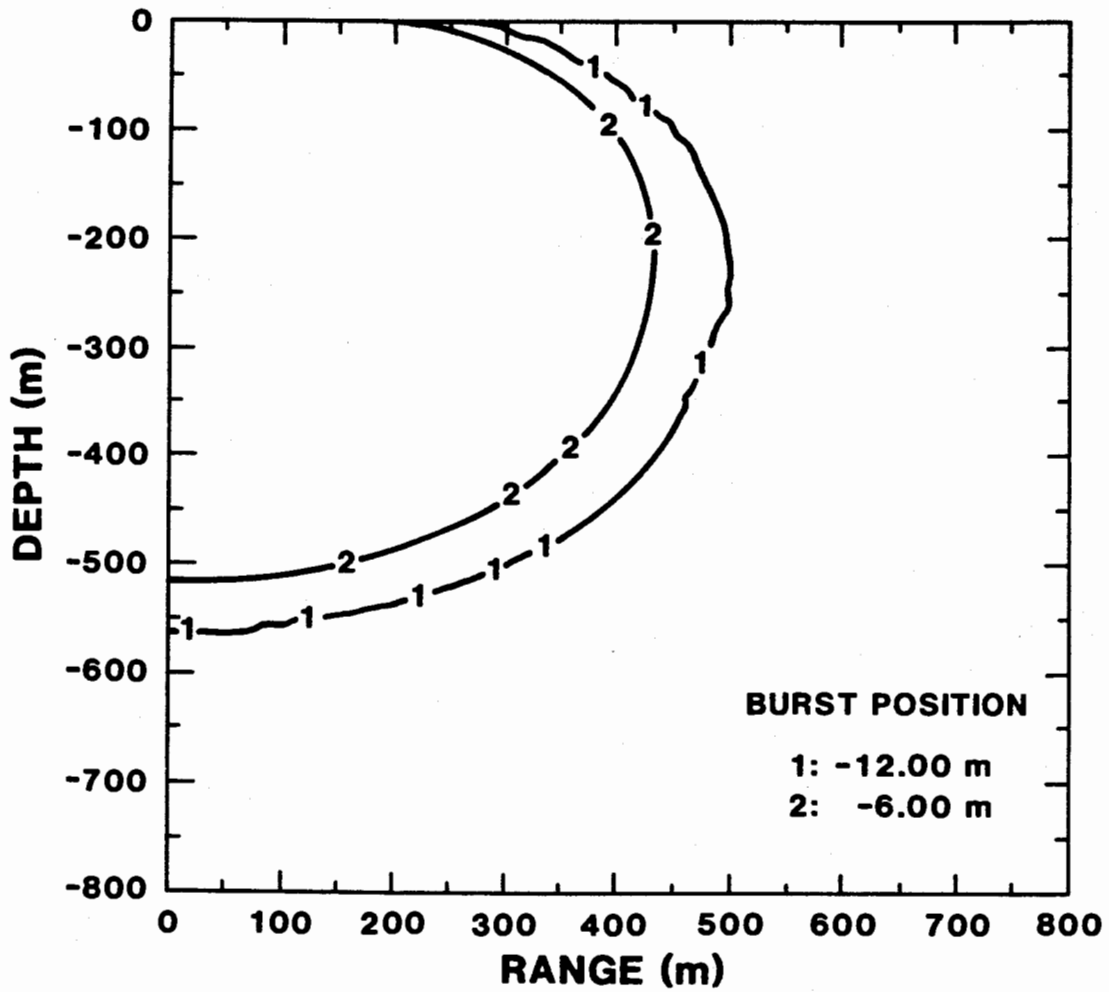


Figure 19: Comparison of 0.5 kb peak horizontal stress contours for EPW bursts.

## 5. Discussion

In this report, we have used cube-root scaling to determine EPW yield factors from differences in ground shock lethal range between surface and buried bursts. The results show enhancements in ground shock effects for earth penetrating weapons that are considerably larger than would be predicted using standard *empirical* methodologies. In Ref. [7], for example, the "equivalent yield coupling factor" for an EPW "shallow burst" is estimated to be 4 times that of a contact burst. No guidance is provided, however, on what constitutes a "shallow burst" or how the coupling factor might vary with depth of burst. In the present calculations, it was seen that a 500 kt EPW at 6 meters DOB has a yield factor of 12 relative to a contact burst, while an EPW at 12 meters DOB has a yield factor of 18 (more than 4 times larger than that given in [7]).

It should be noted that we modeled a homogeneous, saturated target geology in these calculations. This material was relatively non-dissipative to the ground shock from any of the bursts. Actual target geologies, however, are likely to include several meters of soft, somewhat porous soil near the ground surface, which would be quite effective in dissipating shock waves. The ground shock from a surface burst, in particular, would be rapidly attenuated as it propagated through this material. An EPW, on the other hand, would be expected to penetrate soft surface layers before coming to rest. As a result, the ground shock from the EPW would need to travel through much less of the soft material, and would dissipate a much smaller fraction of its energy, before reaching the harder, deeper layers of the target geology. Therefore, in more realistic geologies, the relative effectiveness (yield factor) of an EPW for delivering ground shock could be even larger than predicted by the calculations reported here.

## 6. Acknowledgements

The author wishes to acknowledge the calculational support of D. M. Webb (retired - formerly 1533) on this project and the useful comments of T. K. Bergstresser (1531) and R. A. Paulsen (9013) as reviewers of the report.

## 7. References

1. Davey, W. R. and P. Yarrington, "Weapon Effects Calculations for High-Yield Nuclear Proximity and Contact Bursts (U)," SAND88-0569 (to be released).
2. Farnsworth, A. V., "Relative Effectiveness of a Shallow, Earth Penetrating Nuclear Weapon," SAND88-0868 (to be released).
3. Thompson, S. L., "CSQII - An Eulerian Finite Difference Program for Two-Dimensional Material Response," SAND77-1339, 1/79 (Reprinted 6/85).
4. Thompson, S. L. and H. S. Lauson, "Improvements in the Chart-D Radiation-Hydrodynamics Code III: Revised Analytic Equations of State," SC-RR-71 0714, 3/72 (Reprinted 2/84).
5. Bergstresser, T. K., et al, "Nuclear Explosion Height-of-Burst Study," SAND80-2358, 3/83 (SRD).
6. Memo, W. T. Brown to P. Yarrington, "Spherically Symmetric Explosion in Tuff," dtd. 8/11/87.
7. Crawford, R. E., et al, "The Air Force Manual for Design and Analysis of Hardened Structures," AFWL-TR-74-102, 10/74 (Ninth Printing 2/80).

### APPENDIX

#### A. ANEOS Input for Saturated Tuff

```

-----1-----2-----3-----4-----5-----6-----7
-2
TUFF
1.00      4.00      2.00      0.00      0.00      -2.80E+05      1.00
1.01      2.00      1.00E+11      0.11
1.20
9.0  1.0

```

```

-----1-----2-----3-----4-----5-----6-----7

```

#### B. CSQII updates to provide pressure-dependent strength model for tuff

```

*ID PAULS
*I EP.716
YVSPT1=1.49E11*(RHOI(L)-2.0)
YVSPT2=0.30-0.30*EXP(-3.1E-09*YVSPT1)
YVSPT2=1.0E9*YVSPT2
IF(L.EQ.2)YOFMAT=AMIN1(YOFMAT,YVSPT2)
YOFMAT=AMAX1(YOFMAT,0.0)

```

#### C. CSQGEN/CSQII updates to save ground shock quantities in mesh

##### C.1 CSQGEN updates

```

*ID MORST
*I GIIR.4
C IMPULSE, PEAK STRESS, AND PEAK VELOCITY UPDATES FOR CSQGEN
NVAR=NVAR+1
LK21=NVAR
NVAR=NVAR+1
LK22=NVAR

NVAR=NVAR+1

```

LK23=NVAR  
NVAR=NVAR+1  
LK24=NVAR  
NVAR=NVAR+1  
LK25=NVAR

\*I CSQGEN.315

C LABELS FOR LINE PRINTER LISTING. NEED TO SET NEXTV1,NEXTV2,  
C OR NEXTV3 TO 21-25(YOUR CHOICE) ON CARD 4 OF CSQGEN INPUT.  
IF(L2.EQ.21) KLAB(I)=6HIMPULS  
IF(L2.EQ.22) KLAB(I)=6HMAXSY

IF(L2.EQ.23) KLAB(I)=6HMAXSXX  
IF(L2.EQ.24) KLAB(I)=6HMAXVY  
IF(L2.EQ.25) KLAB(I)=6HMAXVX

\*I CSQGEN.924

STORE(JVAR+LK21)=(AMR\*STORE(JVAR+LK21)+ANS\*FITS(5,2))/AMT  
STORE(JVAR+LK22)=(AMR\*STORE(JVAR+LK22)+ANS\*FITS(5,3))/AMT  
STORE(JVAR+LK23)=(AMR\*STORE(JVAR+LK23)+ANS\*FITS(5,4))/AMT  
STORE(JVAR+LK24)=(AMR\*STORE(JVAR+LK24)+ANS\*FITS(5,5))/AMT  
STORE(JVAR+LK25)=(AMR\*STORE(JVAR+LK25)+ANS\*FITS(5,6))/AMT

\*I CSQGEN.2654

C UPDATES FOR SUBROUTINE REZONE

IF(IK.NE.94) GO TO 201  
DUM1=DUMMY(1)  
DUM2=DUMMY(2)  
DUM3=DUMMY(3)  
DUM4=DUMMY(4)  
DUM5=DUMMY(5)  
DUMMY(1)=STORE(JVAR+LK21)  
DUMMY(2)=STORE(JVAR+LK22)  
DUMMY(3)=STORE(JVAR+LK23)  
DUMMY(4)=STORE(JVAR+LK24)

DUMMY(5)=STORE(JVAR+LK25)  
201 IF(IK.NE.95) GO TO 202  
DUMMY(1)=DUM1  
DUMMY(2)=DUM2  
DUMMY(3)=DUM3  
  
DUMMY(4)=DUM4  
DUMMY(5)=DUM5

202 CONTINUE

C.1 CSQII updates

\*ID XTRAV  
\*I CSQ.1510  
C UPDATES FOR CSQ

STORE(JVAR+LK21)=STORE(JVAR+LK21) + PZ\*DT  
SIGYYM=STORE(JVAR+LK22)  
SIGYY=PZ-STORE(JVAR+LK16)  
STORE(JVAR+LK22)=AMAX1(SIGYYM,SIGYY)  
SIGXXM=STORE(JVAR+LK23)  
SIGXX=PZ-STORE(JVAR+LK14)  
STORE(JVAR+LK23)=AMAX1(SIGXXM,SIGXX)  
VYMAX=STORE(JVAR+LK24)  
VYABS=ABS(VB)  
STORE(JVAR+LK24)=AMAX1(VYMAX,VYABS)  
VXMAX=STORE(JVAR+LK25)

VXABS=ABS(VL)  
STORE(JVAR+LK25)=AMAX1(VXMAX,VXABS)

I EP.716

YVSPT1=1.49E11\*(RHOI(L)-2.0)  
YVSPT2=0.30-0.30\*EXP(-3.1E-09\*YVSPT1)  
YVSPT2=1.0E9\*YVSPT2  
IF(L.EQ.2)YOFMAT=AMIN1(YOFMAT,YVSPT2)  
YOFMAT=AMAX1(YOFMAT,0.0)

**EXTERNAL DISTRIBUTION:**

Los Alamos National Laboratory (4)  
ATTN: T. Dey, ESS-5, MS F665  
R. Deupree, ESS-5, MS F665  
R. Weaver, X-2, MS B220  
T. Dowler, S-6, MS F601  
P. O. Box 1663  
Los Alamos, NM 87545

Lawrence Livermore National  
Laboratory (2)  
ATTN: R. Swift, MS L-200  
K. Rosenkilde, MS L-81  
P. O. Box 808  
Livermore, CA 94550

R & D Associates  
ATTN: J. Lewis  
P. O. Box 9295  
Marina del Rey, CA 90295

California Research & Technology (2)  
ATTN: A. Frederickson  
K. Kreyenhagen  
20943 Devonshire St.  
Chatsworth, CA 91311

Pacifica Technology  
Div. of Science Applications  
ATTN: R. Allen  
P. O. Box 148  
Del Mar, CA 92014

S-Cubed  
Division of Maxwell Labs  
ATTN: K. D. Pyatt  
P. O. Box 1620  
La Jolla, CA 92038-1620

Defense Nuclear Agency (2)  
ATTN: SSAB, C. McFarland  
SSAB, M. Pelkey  
Washington, DC 20305

**Sandia Internal:**

- 1510 J. W. Nunziato
- 1520 L. W. Davison
- 1530 D. B. Hayes
- 1531 S. L. Thompson
- 1531 T. K. Bergstresser
- 1533 P. Yarrington (10)
- 1533 W. T. Brown
- 1533 W. R. Davey
- 1533 A. V. Farnsworth
- 1550 C. W. Peterson
- 2300 J. L. Wirth
- 3141 S. A. Landenberger (5)
- 3151 W. I. Klein (3)
- 5110 C. C. Burks
- 5111 D. L. McCoy
- 5112 L. J. Merrill
- 5120 W. R. Reynolds
- 5160 G. R. Otey
- 5161 K. D. Nokes
- 5161 J. A. Anderson
- 5161 A. B. Cox
- 5161 J. E. Gronager
- 5165 S. D. Meyer
- 5165 W. J. Patterson
- 5166 R. C. Hartwig
- 7112 A. J. Chabai
- 8150 J. B. Wright
- 8152 J. C. Swearngen
- 8524 J. A. Wackerly
- 9010 W. C. Hines
- 9013 W. H. Ling
- 9013 R. A. Paulsen
- 9120 M. M. Newsom
- 9122 R. H. Braasch

